Pergamon

Int. J. Heat Mass Transfer. Vol. 38, No. 8, pp. 1457 1466, 1995

0017 9310/95 $9.50+0.00

0017–9310(94)00272–X

Experimental investigation of the mode of phase dissociation in superheated liquid jets

E. MHINA PETER, AKIRA TAKIMOTO and YUJIRO HAYASHI

Department of Mechanical Systems Engineering, Kanazawa University, Kodatsuno 2-40-20, Kanazawa 920, Japan

(*Received* 19 *May* 1994 *and in final form* 22 *July* 1994)

Abstract—The present paper gives an exclusive experimental coverage of the flashing process of pure and gas-associated solutions of water at low absolute pressures. The analyses include the phenomenon of bubble nucleation, growth and departure from the source, and the consequential properties of the flashing and disintegration of the liquid jet. The influence of dissolvable substances in the liquid on the bubble nucleation and altered liquid jet physical properties is also made clear. The outcome of the results also leads to the conclusion that, at high concentrations of the solute gas, dissociative bubble nucleation dominates the process and is associated with simultaneous bubble nucleation at the solid body–liquid interface and in the bulk of the liquid, especially at low liquid temperatures.

1. INTRODUCTION

Flashing phenomena are commonly observed occurrences which take place when a liquid's temperature exceeds a certain degree of superheat. The phenomena can be manifested in the chemical and process plants where liquid superheat is essential. Although the phenomena have positive applications in many engineering processes, they have equal disadvantages in some processes, such as nuclear reactor cooling systems, which are a potential source of nuclear accidents. The positive and negative contributions of the phenomena to engineering processes necessitated further concentration of the study, which could lead to a better understanding of the total phenomena and hence improvement of applications for effective utilization can be achieved.

Major problems encountered during the analysis were related to the initial stages of the liquid flashing process, which govern the following events in the case of the flowing liquid. Other critical problems include the three-dimensional two-phase flow heat transfer and the local momentum transients, which could not be experimentally determined up to now. The difficulties arising from the complexity of the phenomena led to the indirect experimental approach, which in the long run is thought to predict occurrences in the initial stages of the flashing by observing the accompanying activities downstream when the thermodynamic and physical parameters of the system are altered. Some of the outstanding experiments related to the above problems include the ones conducted by Balitskiy and Shurchkova [1], Yatabe and Westwater [2], Mhina Peter *et al.* [3, 4], and Miyatake *et al.* [5–7]. In addition to the observation of the changes occurring downstream, experiments on the simplified isolated cases of a thermodynamic event, e.g. single bubble growth under static or dynamic liquid conditions, were conducted. The outcome of the basic experiments paved the way for the development of simple mathematical models which could accurately predict the mode of occurrence and the development of flashing phenomena, like the ones established by Foster and Zuber [8], Scriven [9], Ishii [10], Jones [11], Kocamustafaogullari and Ishii [12], Riznic and Ishii [13], Jones and Shin [14], and Abuaf *et al.* [15], whose magnificent work is now a benchmark. With the exception of a few research works, most of the works mentioned were conducted for/under high pressure liquid systems.

In the present paper more extensive experimental work on the flashing process of pure liquid water is provided. Unlike the previous experiments [3, 4], the present experimental report gives more detailed data on the bubble nucleation and growth inside a glass tube or nozzle, the two-dimensional distribution of the droplet size and number, and the volumetric flowrate for the case of gas-free pure liquid water. The present results also reveal the extent of the influence of dissolved gases on the inception of flashing and the resulting properties of the shattering liquid jet.

2. REVIEW OF THE BASIC THEORY

The problem of flashing and consequently the shattering of a liquid jet is characterized by the mode of initiation of the nucleation activity of the bubble and the succeeding heat and mass transfer processes, and the local pressure variations at the liquid–vapour interface, which govern the respective bubble growth. The treatment of the heat and mass transfer problem becomes more complex when the effect of the local turbulence and eddies is considered. However, the

NOMENCLATURE

A	unit area
$1/A_i$	interfacial area density
A_z	cross-sectional area of the coherent liquid flow
d	diameter of the dispersed droplet
Δd	droplet diameter interval
d_{32}	Sauter diameter (volume/surface mean diameter)
Fr	fraction number of droplets
g	acceleration due to gravity
h	enthalpy
L	length
n	local droplet number density
N_{80}	mean droplet number density for a jet cross-section with radius equals 80 mm
p	absolute pressure
Δp	pressure difference
$\dot{q}$	rate of heat flow
R	radial coordinate of the liquid flow
T	temperature
t	time
ΔT	temperature difference
U	velocity
U_{le}	effective velocity of the liquid fraction that externally evaporates or dissociates from the main flow
V	volumetric flow-rate
Z	axial location of the flow from the nozzle exit
z	axial location of the flow from the nozzle inlet.

Greek symbols

Γ	external surface or wall shear
ε	volume fraction of the externally evaporated liquid
κ	volume fraction of the internally evaporated liquid
ρ	density.

Subscripts

in	inlet
l	liquid
li	interfacial, liquid side
N	nozzle
R	radial location
s	superheat
sat	saturation
v	vapour
vi	interfacial, vapour side
∞	surrounding (flashing chamber).

problem is considerably enlightened if the approach is restricted on the macroscale or averaged values.

By utilizing Ishii's [10] concept of the one-dimensional energy conservation equations for gas–liquid flows, the following secondary equations are developed for the liquid–vapour mixture flowing inside the pipe or the free jet emitted from the flashing chamber.

Conservation of mass

$$\frac{\partial}{\partial t}((1-\kappa-\varepsilon)\rho_l+\kappa\rho_v)+\frac{\partial}{\partial z}((1-\kappa)\rho_l U_l-\varepsilon\rho_l U_{le}+\kappa\rho_v U_v)+((1-\kappa)\rho_l U_l-\varepsilon\rho_l U_{le}+\kappa\rho_v U_v)\frac{1}{A_z}\frac{dA_z}{dz}=0. \quad (1)$$

Conservation of linear momentum

$$\frac{\partial}{\partial t}((1-\kappa)\rho_l U_l-\varepsilon\rho_l U_{le}+\kappa\rho_v U_v)+\frac{\partial}{\partial z}((1-\kappa)\rho_l U_l^2-\varepsilon\rho_l+U_{le}^2+\kappa\rho_v U_v^2)=(1-\kappa-\varepsilon)\frac{\partial p_l}{\partial z}+\kappa\frac{\partial p_v}{\partial z}-\Delta p_l\frac{\partial(1-\kappa-\varepsilon)}{\partial z}+\Delta p_v\frac{\partial\kappa}{\partial z}+(1-\kappa-\varepsilon)\rho_l g\cos\theta+\kappa\rho_v g\cos\theta-\Gamma_l-\Gamma_v. \quad (2)$$

Conservation of energy

$$\frac{\partial}{\partial t}((1-\kappa-\varepsilon)\rho_l h_l+\kappa\rho_v h_v)+\frac{\partial}{\partial z}((1-\kappa)\rho_l U_l h_l-\varepsilon\rho_l U_{le}h_{le}+\kappa\rho_v U_v h_v)=(1-\kappa-\varepsilon)\left(\frac{\partial p_l}{\partial t}+U_l\frac{\partial p_l}{\partial z}\right)+\kappa\left(\frac{\partial p_v}{\partial t}+U_v\frac{\partial p_v}{\partial z}\right)-U_l\Gamma_l-U_v\Gamma_v+\frac{\dot{q}_{li}+\dot{q}_{vi}}{A_i}. \quad (3)$$

In this paper the above equations have been accordingly applied to back up theoretical explanations which interrelate some of the occurrences observed during experimentation.

3. EXPERIMENTAL APPARATUS AND METHOD

The main experimental equipment consists of the flashing chamber, whose dimensions are as shown in Fig. 1. Flashing chamber pressure was controlled by varying the rate of evacuation of vacuum pumps, which were connected to the flashing chamber via a condenser and anti-carryover, arranged in the same manner as the ones indicated in the previous report [3, 4]. The consequential flashing liquid properties were analysed by conducting both visual observation and measurement inside the flashing chamber. Most of the experimental precautions undertaken in the previous experiments were also considered.

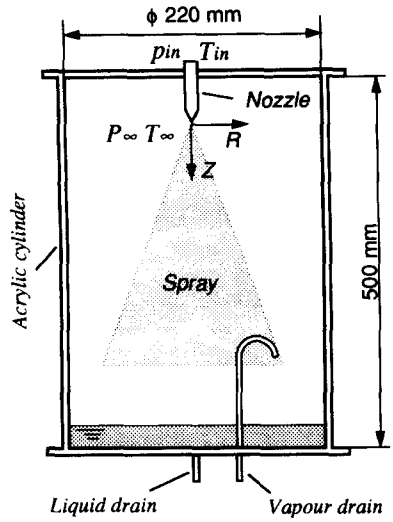

Fig. 1. Flashing chamber.

Measurements of the bubble nucleation and growth were conducted along the smooth-surfaced 500 mm long and 3 mm diameter glass tube, whose one end was connected to the flashing chamber. General features of the glass tube are as indicated in Fig. 2(a). Initial conditions for the bubble nucleation and growth inside the glass tube were determined by controlling the inlet water temperature and the flashing chamber pressure. In all cases the inlet water pressure was maintained at nearly atmospheric conditions during the execution of all experiments.

Post-shattering liquid properties were determined by measuring various quantities of the dispersed droplets downstream from the nozzle outlet. In order to have a good comparison with the previously reported data, in many cases measurements were conducted at the same axial locations as reported previously [3, 4]. However, measurements were also conducted along the plane perpendicular to the flow direction. The axial location at which measurements were conducted was fixed at the point 150 mm downstream from the nozzle outlet. All measurements were taken for the smooth cylindrical glass nozzle having 100 mm length and 1 mm inner diameter; refer to Fig. 2(b).

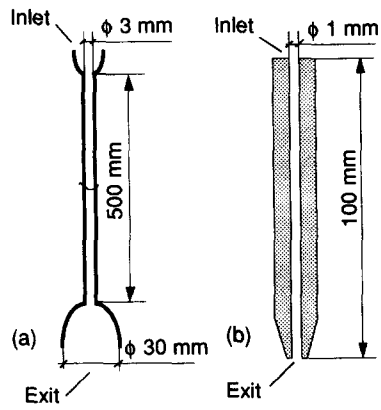

Fig. 2. General features of the glass tube and nozzle.

The experimental apparatus and method varied from one type of experiment to the other. However, the liquid water preparatory procedures were the same. In addition to the distillation process, the distillate was then reboiled at atmospheric conditions in the absence of air for more than half an hour in order to discard gaseous solutes which could have intruded during distillation.

In order to establish the influence of gaseous solutes in the liquid on the flashing behaviour, experiments were also conducted with carbon dioxide–water solutions. Although the maintenance of the given molar concentration of the solution constituents was not critically considered, an effort was made to maintain the solution at near saturation for the given inlet water temperature at atmospheric conditions. Initial introduction of CO_2 in water was pursued by dipping dry ice (CO_2 blocks) in a partially closed container having pure water at a capacity volume of about 30 l (0.03 m^3). A total amount of about 5 kg of solid ice was introduced in each round and left to sublime slowly while cooling the water and partly dissolving in it. To affirm the saturated condition of water during experimentation, the inlet water temperature was maintained at higher levels than the initial water temperature immediately after the formation of the solution. At higher liquid temperatures (above 50°C), reimmersion of dry ice in the solution was necessary to compensate for the dissociated carbon dioxide during heating.

The droplet size distribution pattern along the plane perpendicular to the flow was determined by trapping incoming droplets at given locations on the plane. The liquid droplet trapping method employed was applying silicone oil, which is pasted on top of a glass slide. By controlling the shatter speed the resulting number of droplets which impinge on the silicone oil surface per unit area is determined. There were nine sampling locations linearly aligned with an interspace distance of 10 mm and the sampling area for each chosen location is circular with radius of 3 mm. In order to differentiate the sampling locations from the others, the rest of the glass slide was shaded.

Likewise, the volumetric flow-rate distribution was determined by trapping droplets inside the honeycomb-like measuring device having 10 pots with a rectangular prism shape. The mouth of each pot was square shaped with the dimensions 10×10 mm, having wedge shaped end-walls to minimize partition or end error. Reduction in surface area of the liquid trapping pots was pursued in order to increase the accuracy of measurements compared to the similar ones reported earlier [3, 4]. The liquid influx was within the same range as that reported in the previous experiments [4], i.e. of the order of 5.0×10^{-6} m^3 s^{-1}, which is equivalent to an inlet liquid velocity of about 6 m s^{-1} for a 1 mm diameter nozzle. The small variation of the amount of the liquid influx for a given

nozzle and thermodynamic conditions considered during experimentation enabled the negation of the velocity factor when comparing the respective results. The uncertainty in the value of the volumetric flow-rate is estimated to be $\pm 5\%$.

4. RESULTS AND DISCUSSION

The results due to visual observations of the glass tube [Fig. 2(a)] reveal that the bubble nucleation for pure liquid water occurs heterogenically on the wall surface of the smooth glass tube for the given range of inlet water temperature, pressure and liquid velocity. A closer look at nuclei unveiled the fact that, for a given active bubble source, there is no instance at which the nucleus is completely displaced by water. That means there is a continuous presence of a vapour nucleus at the active nucleation centre on the wall surface. The presence of micro-cavities or pits formed naturally on the nozzle surface during manufacturing may be the reason for the existence of the respective active bubble nucleation centres [16].

The results regarding the measurements of the effect of changing thermodynamic conditions of the system on the bubble nucleation and departure have shown that, depending on the liquid velocity inside the tube, bubbles can be heterogeneously nucleated on the wall even under the local liquid subcooled conditions. Sporadic release of vapour bubbles from the wall surface is attainable even at the extremely high subcooled conditions, while steady departure of the bubbles is attained at near equilibrium conditions.

Initial conditions for the sporadic and steady bubble generation, and departure inside the glass tube for the given thermodynamic conditions are respectively displayed in Fig. 3(a) and (b). The degree of superheat ΔT_s displayed in Fig. 3(b) is calculated as per the following equation:

$$\Delta T_s = T_{in} - T_{sat}(p_\infty). \quad (4)$$

The initial bubble growth and departure could be activated under the subcooled liquid conditions for both cases. Even though the bubbles could be generated steadily from their source, no noticeable growth of the released bubbles was traced downstream. The occurrence may suggest that, apart from the premature departure of bubbles from their source, due to the sweeping effect of the flowing liquid around the nucleated bubble, local pressure variations or perturbations around the nucleus may undeniably have contributed to the initial growth of the bubble predeparture, since a certain degree of superheat is necessary to achieve the growth of the bubble as described by the Kelvin theory. The non-growing bubble release was also substantiated by the fact that the liquid jet did not shatter, although the churning effect could be observed. This condition can be aptly related to the non-shattering liquid jet condition [3, 4]. Unlike the case of bubble departure in very small diameter nozzles, e.g. 1 mm diameter nozzle, where direct visual

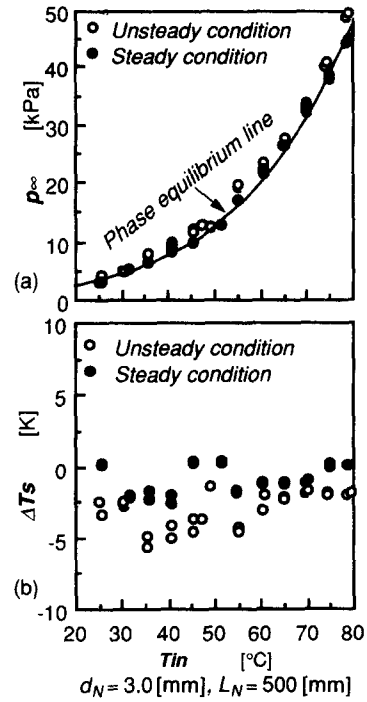

Fig. 3. Initial conditions for the bubble nucleation and departure for gas-free pure water.

observation of bubbles was impossible, and only the sparkling and churning of the released liquid jet allowed speculation of the presence of bubbles in the liquid jet, the initial conditions for the similar observations could be detected under the liquid subcooled conditions. From that observation, one may conclude that, although the degree of pressure perturbation at a location appears to be independent of the tube or channel diameter at larger diameters, as reported previously [9], it may be strongly influenced by the same parameter for smaller tube diameters. That is, the degree of perturbation may be positively decreased with the increase in the respective diameter of the channel or the tube. The corresponding data for the initial conditions for the bubble departure and growth in the case of pure water and carbon dioxide–water solution for the small diameter nozzle (1 mm diameter nozzle) are displayed in Fig. 4. The uncertainty in the value of ΔT_s, brought about by both the instrumental reading error and the possible local pressure difference due to the air leakage into the flashing chamber, and the evaporation and discharge of carbon dioxide at the liquid–vapour interface, is estimated to be about ± 0.5 K.

Since direct measurements of the individual bubble size change were not possible, the general physical characteristic change of the jet was the reference parameter. As mentioned in the former report [3, 4], with regard to the physical characteristics of the flashing liquid jets, in which four major characteristic configurations of the superheated liquid jet were disclosed, namely non-shattering liquid jet, partially

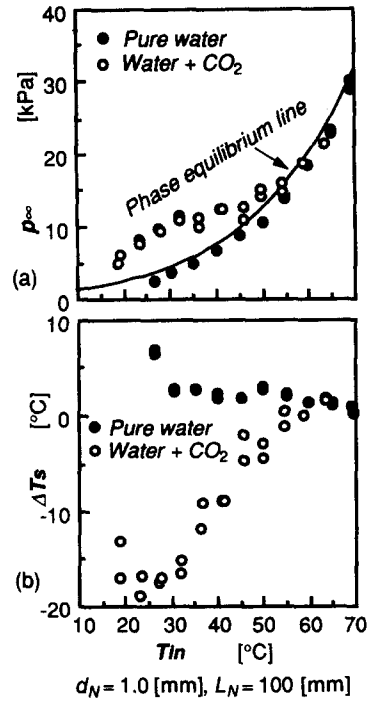

Fig. 4. Comparison between the initial conditions necessary for triggering bubble nucleation and departure between pure water and water + CO_2 solution.

shattering liquid jet retaining the inner core, stagewise shattering liquid jet and the flare flashing liquid jet, minimum conditions for bubble departure and growth were determined to lie between the first and the second type of the flashing liquid jet, i.e. a transition state to stage two. The transition state to the second type of the flashing liquid jet is characterized by the formation of the distinct form of the liquid jet. Under this state, the liquid jet forms a node downstream which is the result of the thickening and later thinning of the liquid jet column. The described phenomenon is illustrated diagramatically in Fig. 5(a). Some detached liquid ligaments which might have emerged from the weakly rupturing bubbles at the maximum expansion point could be observed downstream. The formation of the

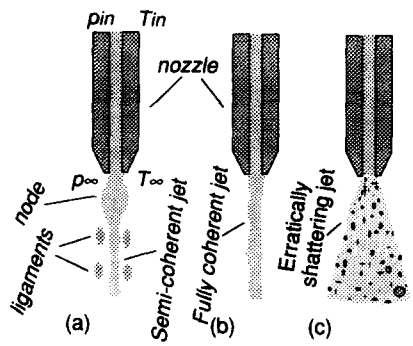

Fig. 5. Liquid jet configurations: (a) node formation; (b) non-shattering jet; (c) flare flashing.

node is predicted to be the outcome of the gross expansion of bubbles near the critical conditions. In the course of expansion, bubbles absorb vapour from the surrounding liquid which, in addition to other external heat loss, e.g. due to evaporation, decreases in temperature. The condition regarding the above problem of heat transfer and energy balance has been described in simplified form in equation (3). Depending on the difference of the bubble growth rate and the net drop in liquid temperature, the bubbles may grow or collapse. If the net growth of the bubbles is negative, thinning of the jet occurs, i.e. the value of κ applied in equations (1)–(3) decreases in magnitude, otherwise the jet thickness continues to grow until reaching the total jet disintegration point. This state of liquid condition is easily attainable in the small diameter jets compared to the large diameter jets due to the difficulties accruing from the limited external surface area for the heat transfer in thick jets: thus it is very likely not to be clearly visible in the case of the large diameter nozzles. However, up to this point, no experiments on the larger jet diameters aimed at ascertaining the above argument have been executed.

On the other hand, the initial bubble growth for the carbon dioxide–water solution could not be determined by observing the node formation, since under this situation the bubble number density was very high, probably due to the simultaneous nucleation on the wall surface and the bulk of the liquid. Also, unlike the case of pure water, the conditions for the bubble collapse or reverse action could not be attained, since pressure inside the flashing chamber was very much lower than atmospheric pressure and the liquid temperature drop could not exceed the saturated point. Therefore, minimum conditions were determined when the jet just began to loose its coherence, characterized by the formation of ligaments downstream. In the present analysis, only two types of liquid jet configurations for the carbon dioxide–water solution jet have been distinguished, namely, non-shattering liquid jet [Fig. 5(b)] and flare flashing liquid jet [Fig. 5(c)]. The present finding is in contrary to the one reported [3, 4] for pure liquid water, where four basic categories of liquid jet were determined. In the latest case, when the degree of liquid superheat is increased at constant inlet liquid pressure and flashing chamber pressure, the liquid jet directly transforms from the fully coherent state to the totally disintegrated liquid jet state just near the nozzle exit. This typical behaviour emphasizes the occurrence of the sudden increase in the rate of bubble nucleation on the wall surface and the bulk of the liquid governed by the solute–gas dissociation. That means that the magnitude of the void fraction κ becomes greater than the limiting value for the maintenance of the liquid flow continuity before/when reaching the nozzle exit. However, since the degree of dispersion of the droplets depends on the rate of expansion of the bubbles, which in turn depends on the available energy and the rate of heat transfer at the interfaces [equation (3)], the

angle of dispersion of the droplets, as expected, increases with the increase in the degree of superheat of the solution at a constant flashing chamber pressure.

The displayed results in Fig. 4 reveal that, at lower liquid temperatures, the conditions for bubble nucleation are generally easily obtained for a carbon dioxide–water solution compared to pure water and they are substantiated by the degree of superheat or subcooling necessary for triggering the phenomenon. The degree of superheat necessary to initialize the bubble nucleation for the solution increases with the increase in water temperature and approaches that of pure water at temperatures close to or above 60°C. Higher degrees of subcooled conditions for triggering nucleation in the solution at lower temperatures are governed by the dominance of dissociative bubble nucleation due to high molar concentrations of the solute gas. At higher temperatures, dissociative bubble nucleation process becomes weaker and the evaporative process becomes more active.

Volumetric flow-rate patterns for the 1 mm diameter nozzle are displayed in Fig. 6. The patterns are basically grouped into three, based on the inlet water temperature. The first group shows variations in the volumetric flow-rate distribution patterns with the change in flashing chamber pressure, when the inlet water temperature is maintained close to 50°C. The second one is for the inlet water temperature range close to 60°C, and the last one is for water at nearly 70°C. In all cases it is clearly visible that the volumetric flow-rate near the central axis of the spray quantitatively decreases with the increase in the flashing chamber pressure at constant inlet water temperature. In other words, the volumetric flow-rate at the central axis of the spray decreases with the increase in the degree of superheat at constant inlet temperature. If the degree of dispersion is compared at constant pressure potentials for both cases of inlet water temperature, it is easily deduced that the degree of dispersion is higher at low temperatures compared to higher water temperatures. This typical characteristic behaviour may be attributed to the nature of the liquid–vapour phase equilibrium curve which indicates that the saturated vapour pressure increases rather parabolically with the increase in liquid temperature. Thus higher degrees of superheat are exhibited at low liquid temperature compared to higher liquid temperature at constant pressure potential. Since the bubble growth rate is positively proportional to the local liquid degree of superheat, and the degree of dispersion of droplets is a function of the rate of expansion of bubbles at the breakup point, then, at constant pressure potential, the degree of dispersion of droplets should be expected to be higher at lower temperatures compared to higher liquid temperatures. Contrary to the previous report [6], where the difference in inlet water temperature was thought not to have a noticeable influence on the temperature distribution patterns when the degree of superheat is

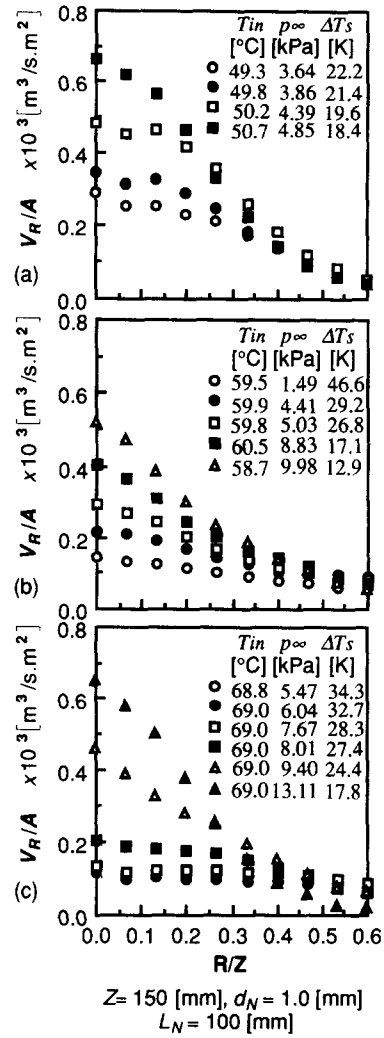

Fig. 6. Volumetric flow-rate distribution for gas-free pure water.

kept constant, like other quantities, some noticeable influence has been detected while undertaking the quantitative assessment in the case of the volumetric flow-rate distribution patterns. The corresponding volumetric flow-rate distribution for a carbon dioxide–water solution is displayed in Fig. 7(a) and (b) for the solution at an inlet temperature close to 50 and 60°C, respectively. Similar to the results depicting minimum onset conditions for bubble nucleation, the distribution trend appears to deviate from that of pure water for an inlet temperature of about 50°C, while at higher liquid temperatures (near or above 60°C) the volumetric flow-rate distribution trend approaches that of pure water both quantitatively and qualitatively. By combining the results regarding the bubble nucleation and departure for pure water and carbon dioxide–water solution displayed in Fig. 4, and the associated explanations included in the preceding paragraphs, it can be concluded that the degree of

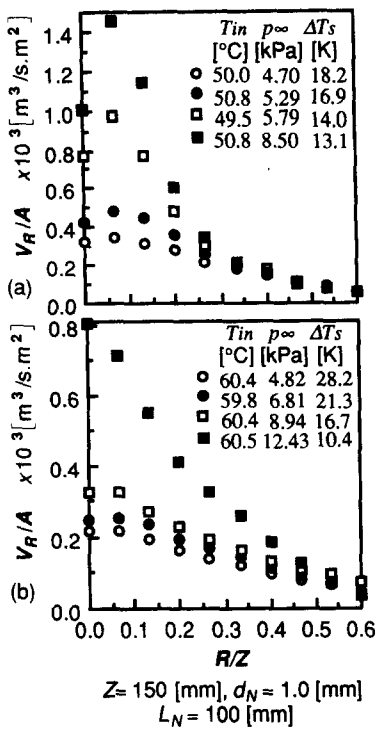

Fig. 7. Volumetric flow-rate distribution for water+CO_2 solution at near saturation.

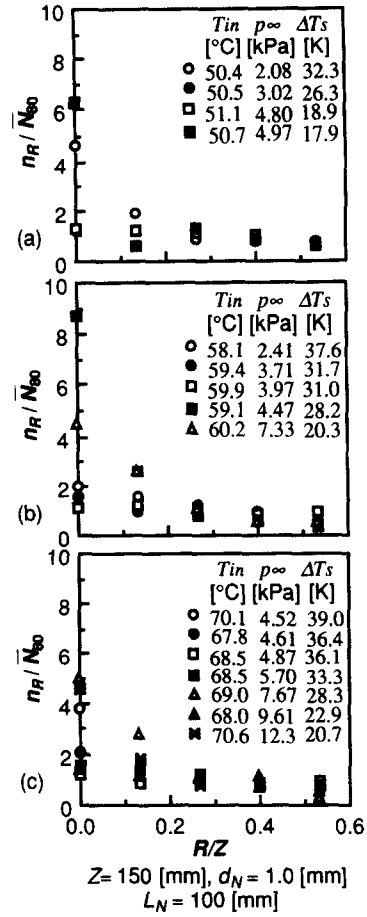

Fig. 8. Relative droplet number density distribution.

divergence in the volumetric flow-rate distribution trend is likely to increase with decreasing inlet water temperature.

The distribution of the relative number density of droplets along the radial direction of the jet axis for the given thermodynamic conditions is shown graphically in Fig. 8(a)–(c), for the inlet water temperature range of 50–70°C. Unlike the absolute number density distribution in which time is also a parameter, the relative number density is the time-independent dimensionless distribution characteristic trend which weighs the local number density distribution against the average droplet number distribution over a predetermined region. For the sake of convenience the pre-determined region lies within the radius of 80 mm from the central axis of the spray. The trend was purposely established to eliminate the factor, which needed a rather complicated shutter to provide accurate measurements. In general, the results show very little difference from one set of data to the other for nearly the whole range of thermodynamic conditions considered during experimentation, apart from the sporadic deviations at the central axis of the spray. Many of the data exhibit the steep decline in the number density near the central axis of the spray and the drop in number density becomes more gradual farther from the central axis.

Droplet size distribution patterns at the selected locations along the plane perpendicular to the flow direction under the given thermodynamic conditions are displayed in Figs. 9–11 for inlet water temperatures close to 50, 60 and 70°C, respectively. As seen in the graphs, the distribution approaches log–normal with the mode of the order of 10 μ. Apart from the data collected from the central axis of the flow, where high mode amplitudes are recorded, it has been generally determined that there is no major difference in the given distribution trends at the locations away from the central axis, at least for the given range of thermodynamic parameters. From the available data, it is not so clear how the change in thermodynamic parameters and the relationship between the location of the sampling points influence the change in size for the largest and smallest diameters, and the amplitude of the mode. The limitations of applying the batch size distribution to predict the real distribution may be attributed to the difficulties arising from applying the displayed results for the accurate description of the trends. High numbers of trapped droplets per given sampling point were favoured, however, due to technical problems mainly attributed to the interference, intermingling or coalition of droplets after impinging on the silicone oil restricted the adjustment of the shatter speed to higher values only. Secondly, due to considerable

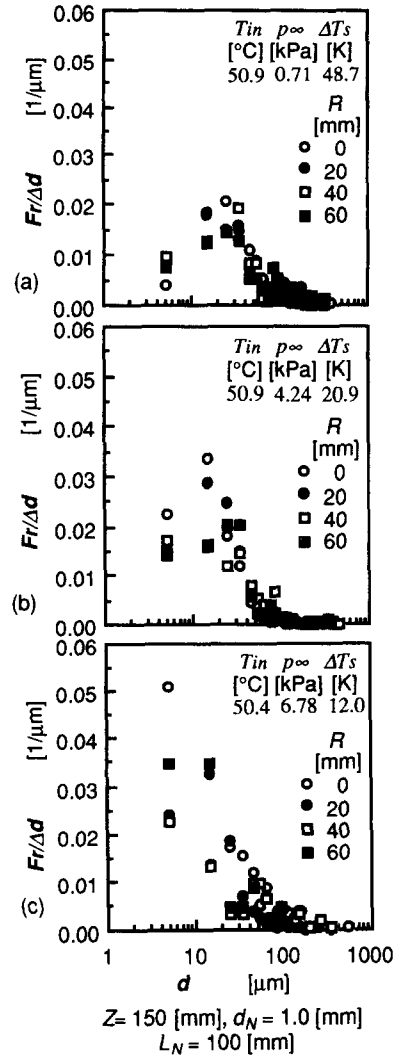

Fig. 9. Droplet size distribution for water at inlet temperature of the order of 50°C.

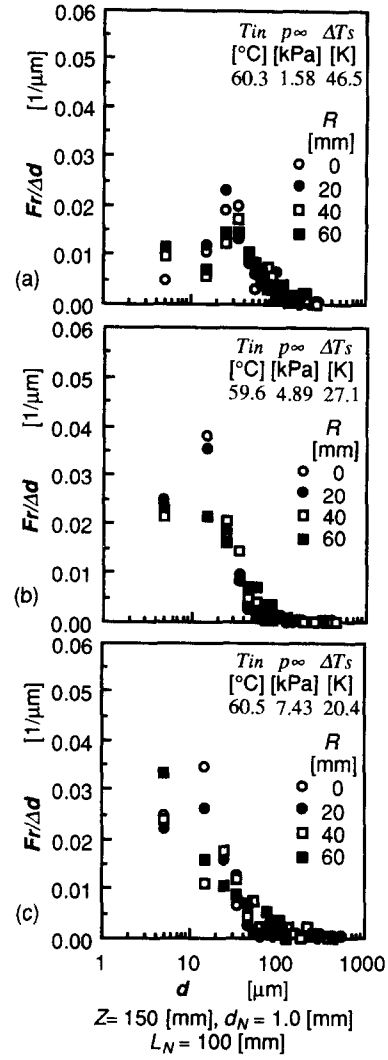

Fig. 10. Droplet size distribution for water at inlet temperature of the order of 60°C.

differences in the droplet number density distribution between the sampling point located at the central axis of the flow and the one in the peripheral region, the number of droplets trapped farther away from the central axis was very small and hence the distribution error is automatically predicted to be higher at those locations.

The distribution of the Sauter diameter as per the batch sampling is delineated in Fig. 12. The graphs exhibit the gradual size enlargement of the Sauter diameter with the location displacement from the central axis of the spray. As mentioned earlier, the authenticity or reliability of the displayed trends for the description of the overall patterns depends on the batch size and the individual size distribution: thus, the displayed patterns are somehow very likely to deviate from the real distribution if the sampling could be continuously undertaken. Unlike the size distribution, the Sauter diameter distribution is critically affected by the respective recorded diameter values away from the mode, especially for the log–normal distribution. It follows that the occurrence of an error amplification is unavoidable under the present approach for data processing.

5. CONCLUSIONS

The consistency of the data gathered on the flashing and shattering of a superheated liquid jet in a low pressure field has paved the way for the development of individual models which may be applied to estimate qualitatively and quantitatively the accruing phenomena. The present results have upgraded the conceptual outlook of the mode of occurrence of the flashing phenomena by extending precisely and conclusively the parametric range under which the data were

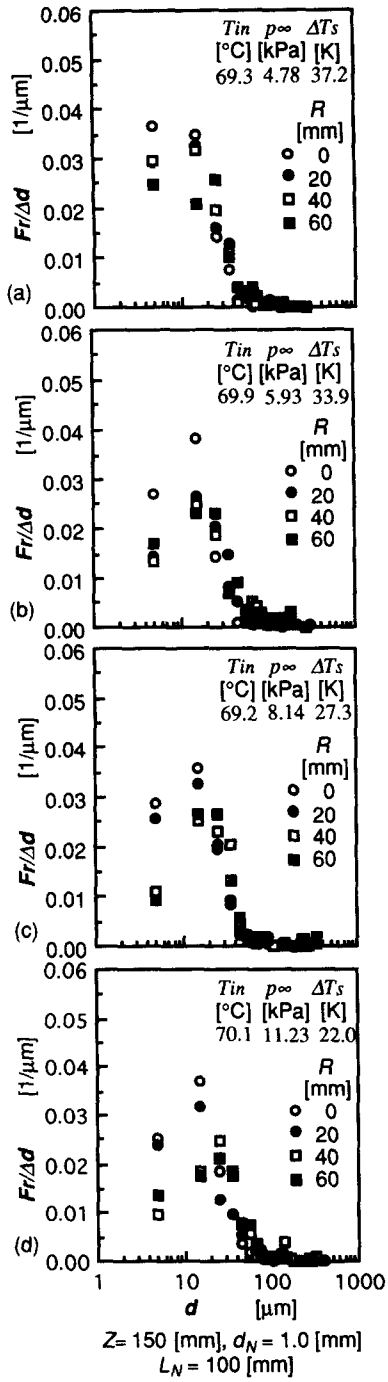

Fig. 11. Droplet size distribution for water at inlet temperature of the order of 70°C.

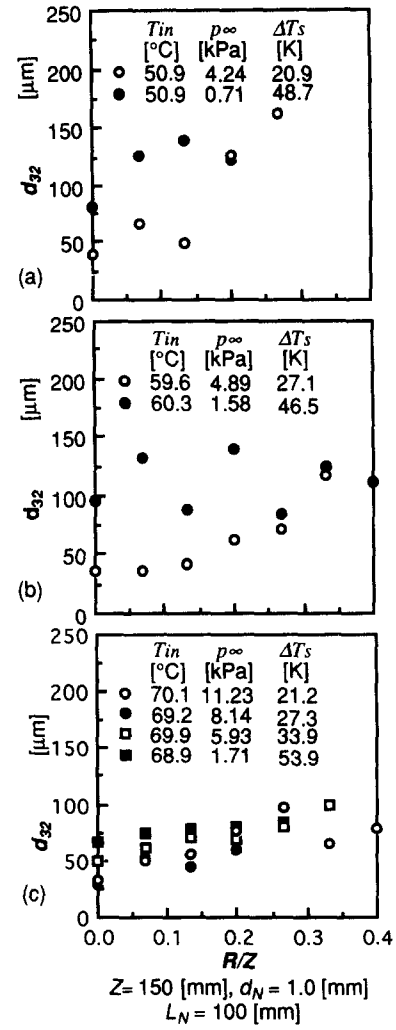

Fig. 12. Sauter diameter distribution along the plane perpendicular to the axis of the flow.

collected, and hence more general theoretical analysis can now be confidently given by combination with the experimental results on high pressure flashing processes previously reported by other authors.

REFERENCES

1. S. A. Balitskiy and Yu. A. Shurchkova, Flashing of the superheated liquid under vacuum, *Heat Transfer Sov. Res.* **1**, 106–109 (1969).
2. J. M. Yatabe and T. W. Westwater, Bubble growth rates for ethanol–water and ethanol–isopropanol mixtures, AICHE, Pre-print, No. 7, *8th National Heat Transfer Conference*, AIChE–ASME, Los Angeles, CA (1965).
3. E. Mhina Peter, A. Takimoto and Y. Hayashi, Mechanism of flashing spray evaporation in decompression fields, *29th National Symposium of Heat and Mass Transfer*, Osaka (1992).
4. E. Mhina Peter, A. Takimoto and Y. Hayashi, Flashing and shattering phenomena of superheated liquid jets, *JSME Int. J.* **37**, 313–321 (1994).
5. O. Miyatake, T. Tomimura, Y. Ide and T. Fujii, An experimental study of spray flash evaporation, *Desalination* **36**, 113–128 (1981).
6. O. Miyatake, T. Tomimura, Y. Ide, M. Yuda and T. Fujii, Effect of liquid temperature on spray flash evaporation, *Desalination* **37**, 351–366 (1981).
7. O. Miyatake, T. Tomimura and Y. Ide, Enhancement of spray flash evaporation by means of the injection of bubble nuclei, *ASME J. Solar Energy Engng* **107**, 176–182 (1985).
8. H. K. Foster and N. Zuber, Growth of a vapour bubble in a superheated liquid, *J. Appl. Phys.* **25**, 474–478 (1954).
9. L. E. Scriven, On the dynamics of phase growth, *Chem. Engng Sci.* **10**, 1–13 (1959).

10. M. Ishii, *Thermo-fluid Dynamic Theory of Two-phase Flow*. Eyrolles, Paris (1975).
11. O. C. Jones Jr, *Flashing Inception in Flowing Liquids in Non-equilibrium Two-phase Flow*, pp. 29–34. ASME, New York (1979).
12. G. Kocamustafaogullari and M. Ishii, Interfacial area and nucleation site density in boiling systems, *Int. J. Heat Mass Transfer* **26,** 1377–1387 (1983).
13. J. R. Riznic and M. Ishii, Bubble number density and vapour generation in flashing flow, *Int. J. Heat Mass Transfer* **32,** 1821–1833 (1989).
14. O. C. Jones Jr and T. S. Shin, Progress in modelling of flashing inception and critical discharge of initially subcooled liquids through nozzles, *Joint Japan–U.S. Seminar on Two-phase Flow Dynamics*. Lake Placid, New York (1984).
15. N. Abuaf, O. C. Jones Jr and B. J. C. Wu, Critical flashing flows in nozzles with subcooled inlet conditions, *ASME J. Heat Transfer* **105,** 379–383 (1983).
16. J. Frenkel, *Kinetic Theory of Liquids*, p. 373. Dover, New York (1955).